Deciphering age-related differences in wound healing: Insights from the interaction between endothelial cells and fibroblasts

JIANJUN LI[1-3*], DONGZHEN ZHU[1*], MENGDE ZHANG[1], ZHAO LI[1], LITING LIANG[1], YUYAN HUANG[1], XU GUO[4], YI KONG[1], XIAOBING FU[1] and SHA HUANG[1]

[1]Research Center for Tissue Repair and Regeneration Affiliated to the Medical Innovation Research Department, PLA General Hospital and PLA Medical College, PLA Key Laboratory of Tissue Repair and Regenerative Medicine, Beijing 100853, P.R. China; [2]Department of General Surgery, The Six Medical Centre, Chinese PLA General Hospital, Beijing 100853, P.R. China; [3]Department of General Surgery, The First Medical Centre, Chinese PLA General Hospital, Beijing 100853, P.R. China; [4]College of Graduate, Tianjin Medical University, Tianjin 300050 P.R. China

Received February 4, 2025; Accepted July 10, 2025

DOI: 10.3892/mmr.2025.13643

Abstract. Aging impairs wound healing, primarily because of alterations in cell phenotypes and interactions, particularly between endothelial cells (ECs) and fibroblasts (Fibs). The present study investigated the dynamics of EC-Fib interactions in aged wounds using a mouse model and single-cell transcriptomics, supplemented by CellChat analysis and functional validation using *in vitro* co-culture systems. Aged mice exhibited markedly reduced wound healing efficiency and impaired angiogenesis when compared with younger mice, as indicated by hematoxylin and eosin and immunohistochemical staining. Single-cell transcriptomic analysis revealed that the regeneration of ECs and Fibs was delayed in aged wounds. Furthermore, key genes involved in angiogenesis and tissue repair were downregulated, whereas those related to inflammation and aging were upregulated. Integrating CellChat analysis with *in vitro* co-culture validation, it was found that the bidirectional communication between ECs and Fibs, predominantly mediated via the transforming growth factor β pathway, was markedly reduced in aged wounds. These findings underscored the critical role of disrupted cell-cell communication in age-related impaired wound healing, providing mechanistic evidence for potential therapeutic strategies to enhance wound healing in the elderly.

Correspondence to: Professor Xiaobing Fu or Professor Sha Huang, Research Center for Tissue Repair and Regeneration Affiliated to the Medical Innovation Research Department, PLA General Hospital and PLA Medical College, PLA Key Laboratory of Tissue Repair and Regenerative Medicine, 28 Fuxing Road, Haidian, Beijing 100853, P.R. China
E-mail: fuxiaobing@vip.sina.com
E-mail: stellarahuang@sina.com

*Contributed equally

Abbreviations: Mac1, type 1 macrophage; Mac2, type 2 macrophage; Neu, neutrophil; Supra, suprabasal cell; Spin, spinous and granular keratinocyte; Basal, basal keratinocyte; Fib, fibroblast; Epi, epithelial cell; EC, endothelial cell; Fp, papillary fibroblast; Lym, lymphocyte; SMC, smooth muscle cell; Germ, germinative layer cell; Fasc, fascia cell

Key words: aged wound, vascularization, single-cell RNA-seq, cell-cell communication, TGF-β

Introduction

Effective and prompt wound healing, which is crucial for the survival of an organism, involves complex interactions among various cell types, particularly between endothelial cells (ECs) and fibroblasts (Fibs). ECs facilitate angiogenesis, promoting the delivery of oxygen and nutrients to the wound site, eliminate metabolites and release anti-inflammatory factors to regulate the inflammatory response. Fibs play a central role in wound healing by responding to cytokines and cellular signals, which activate collagen secretion essential for wound microenvironment remodeling and timely healing. ECs and Fibs communicate to ensure a conducive healing microenvironment, with ECs inducing phenotypic changes in Fibs, including migration and proliferation, thus influencing wound fibrosis and healing outcomes (1-3).

The implication of vascular EC-Fib interaction in normal wound healing has been intensively investigated; however, the mechanism underlying these interactions and the associated phenotypic changes during wound healing in the elderly remain poorly understood. Aging leads to structural and functional changes in the skin, including thinning of the dermal-epidermal junction, alterations in cell proportions, decreased thermoregulatory capacity and reduced moisture retention (4). Cellular senescence in Fibs, coupled with altered collagen secretion and stress responses, further complicates wound healing in the elderly (5-7). ECs in the elderly exhibit decreased revascularization capacity and enhanced inflammation, contributing to poor healing. Moreover, the skin microenvironment in aged individuals is often pro-inflammatory, characterized by a chronic low-grade inflammatory state

and the infiltration of various inflammatory cytokines such as interleukin (IL)-6, IL-8 and tumor necrosis factor (TNF)-α, which contributes to age-related wound healing impairment (8,9). These age-related chronic low-grade inflammatory states not only directly drive phenotypic alterations in cells, including ECs and Fibs, resulting in dysregulated secretion of vascular factors, impaired angiogenesis and aberrant Fib activation, but also disrupt intercellular communication (10,11). Hence, the precise identification of age-related molecular-level changes in ECs and Fibs and associated shifts in their interaction patterns during wound healing is critical.

Therefore, the present study employed a mouse dorsal wound model to replicate the distinct differences in wound healing between aged and young individuals, focusing on impaired vascularization in aged wounds. It constructed a comprehensive single-cell transcriptomic atlas to explore the dynamic changes in cell types and molecular pathways during the healing process in aged and young wounds. Through computational analysis using CellChat, the present study identified and experimentally confirmed significant age-related alterations in cell-cell communication, particularly the dysregulated crosstalk between vascular ECs and Fibs. The present study systematically delineates age-related differences in the regeneration rates, phenotypic changes and communication patterns of these cell types, providing a novel framework for understanding the mechanisms underlying delayed wound healing in the elderly and revealing potential therapeutic targets.

Materials and methods

Experimental animals. A total of eight wild-type C57BL/6J mice, obtained from Beijing Beiyou Biotechnology Co., Ltd. (batch no. XH202404160001), included five 2-month-old (young; weight: 22±1.2 g) and three 22-month-old (aged; weight: 35±2.3 g) male mice for the present study. Young male mice were randomly housed in groups on more than three per cage, while aged mice were individually housed to prevent potential conflicts. All the experimental animals were raised in the Specific Pathogen Free (SPF) facility, where the breeding environment was maintained at a temperature 22-25˚C, with a humidity range of 50-70%. All mice had free access to food and water. Additionally, the environment was regulated by a 12-h light/dark cycle. The full-thickness skin wound with a diameter of 4 mm was generated on the dorsal skin of mice by biopsy punch, after anesthetized by inhalation of isoflurane (3%). The wound healing progress was measured through digital photography at days 0, 2, 4 and 7, respectively. At the predetermined end of the experiment on day 7, under the same anesthetic conditions, the back skin samples were collected from the wound sites of all mice. Following sample collection, the wounds were dressed and sutured. After incising the back skin and dissecting the subcutaneous tissue, the skin flap was everted to reveal the details of the underlying subcutaneous vascular network, which were then captured using digital photography. All animal experimental procedures were approved by Institutional Animal Care and USE Committee of Chinese PLA General Hospital (Beijing, China; approval no. 2023-407-01) and followed the relevant ethical regulations.

Isolation and culture of mouse primary dermal cells. A total of two wild-type neonatal C57BL/6J male mice (weight: 1.4±0.1 g) were obtained from Beijing Beiyou Biotechnology Co., Ltd. (batch no: XH202504300004). Neonatal mice were euthanized by exposure to carbon dioxide for 1 h and immersed in 75% ethanol for 15 min. Following dorsal skin removal, dermal-epidermal separation was performed. The dermal tissue was minced and digested with 0.25% Type I collagenase at 37˚C for 30 min. The resultant cell suspension was sequentially filtered through a 40-μm nylon mesh, centrifuged at 200 x g for 10 min at room temperature and resuspended in DMEM medium (Gibco; Thermo Fisher Scientific, Inc.). Fibroblasts were maintained at 37˚C/5% CO_2 and passaged at 85% confluence.

For endothelial cell isolation, the initial dermal digestate dermal cells were resuspended in EBM-2 medium supplemented with 1 μl/ml puromycin (MilliporeSigma) and maintained for 3 days under 5% CO_2 at 37˚C. After 72-h selection culture under standard conditions (37˚C/5% CO_2), cells were transitioned to puromycin-free EBM-2 complete medium with medium renewal every 48 h. The cells were passaged when the confluence rate reached 85%.

Establishment of high-glucose-induced fibroblast senescence model. Second-passage mouse primary dermal fibroblasts were subjected to senescence induction through chronic hyperglycemic stimulation. Cells were maintained under standard conditions (37˚C/5% CO_2) in high-glucose DMEM (Gibco; Thermo Fisher Scientific, Inc.) at final concentrations of 25 (control), 50 and 75 mM for 7 days with medium renewed every 48 h.

Transwell-based indirect co-culture system. A Transwell chamber system (cat. no. 3413; Corning, Inc.) was employed to investigate ECs-Fibs interactions. Second-passage ECs were seeded in the upper chambers (0.4 μm pore size) at a density of $2x10^4$ cells/well. In the lower chambers, two fibroblast populations were respectively cultured: High glucose-induced senescent fibroblasts and non-treated second-passage fibroblasts. The co-culture system was maintained in a 1:1 mixture of DMEM (Gibco; Thermo Fisher Scientific, Inc.) and EBM-2 (Lonza Group, Ltd.) under standard conditions (37˚C; 5% CO_2) for 72 h. Fibroblasts from the lower chambers were subsequently harvested for phenotypic characterization.

Immunohistochemistry and immunofluorescence. After being fixed in a 4% paraformaldehyde solution for a 24-h period at room temperature, the wound tissues were subjected to gradient dehydration and paraffin embedding, following standard protocols. Subsequently, the tissues were sectioned into 5-μm-thick slices. Hematoxylin and eosin (H&E) staining was performed in accordance with standard procedures. First, the slides were baked at 60˚C for 2 h. Then, dewaxing was performed in xylene at room temperature twice for 10 min each. This was followed by rehydration through a graded ethanol series (100, 95 and 70%) at room temperature for 3 min each. Next, staining was performed in 10% hematoxylin at room temperature for 10 min. Differentiation was achieved in 1% acid alcohol for 10 sec, followed by bluing in 0.2% ammonia water for 1 min. Counterstaining was done in eosin

Y at room temperature for 1 min. Dehydration was performed through a graded ethanol series (70, 95, and 100%) for 30 sec each, and then clearing was done in xylene twice for 5 min each. Finally, the slides were mounted with resin.

For immunohistochemistry: After antigen retrieval, sections were permeabilized with 0.3% Triton X-100 for 15 min at room temperature, followed by blocking with 5% goat serum (cat. no. SL038; Beijing Solarbio) for 1 h at RT. Sections were incubated with primary antibodies against α-smooth muscle actin (α-SMA; 1:500; cat. no. ab7817; mouse; Abcam) and cluster of differentiation (CD)31 (1:4,000; cat. no. ab281583, rabbit; Abcam) at 4˚C for 18 h, followed by Coralite594-conjugated anti-mouse IgG (1:300; cat. no. SA00013-3; Proteintech Group, Inc.) and Coralite488-conjugated anti-rabbit IgG (1:300; cat. no. SA00013-2; Proteintech Group, Inc.) at RT for 2 h. Nuclei were counterstained with DAPI (cat. no. 0100-20; SouthernBiotech) for 10 min at room temperature and visualized using laser scanning confocal microscopy (SP8 Falcon; Leica Microsystems, Inc.) at 40x magnification.

For immunofluorescence: Post antigen retrieval and blocking, sections were incubated with TGF-β1 (1:500; cat. no. 21898-1-AP, rabbit; Proteintech Group, Inc.) and Anti-Smad2 + Smad3 (1:200; cat. no. ab202445, rabbit; Abcam) antibodies at 4˚C for 18 h, Sections were washed 3x5 min with PBS before incubation with 647-conjugated goat anti-rabbit IgG (1:1,000; cat. no. ab150083; Abcam) for 2 h at RT protected from light. After secondary incubation, sections were washed 3x5 min with PBS. Nuclei were counterstained with DAPI (cat. no. 0100-20; SouthernBiotech) for 10 min at RT. Fluorescent images were captured post-DAPI staining at 40x magnification using confocal microscopy (SP8 Falcon; Leica Microsystems, Inc.).

Reverse transcription-quantitative (RT-q) PCR. Cells were harvested for RNA extraction (1x10^6 cells/ml). Total RNA was extracted from cells using TRIzol® reagent (Invitrogen; Thermo Fisher Scientific, Inc.) according to the manufacturer's protocol. Reverse transcription was performed with the PrimeScript RT reagent kit (Takara Biotechnology Co., Ltd.) following the manufacturer's instructions. The synthesized cDNA was amplified using TB Green Premix Ex Taq II (Takara Biotechnology Co., Ltd.) on a QuantStudio 5 system (Thermo Fisher Scientific, Inc.) with the following cycling conditions: 95˚C for 30 s (initial denaturation); 40 cycles of 95˚C for 5 s (denaturation) and 60˚C for 30 s (annealing/extension) according to the manufacturer's protocol. Gene expression were normalized to GADPH and quantified using the 2-ΔΔCq method (1). These experiments were replicated three times. The primer sequences were: GAPDH: F 5'-AGGTCGGTG TGAACGGATTTG-3'; R 5'-TGTAGACCATGTAGTTGA GGTCA-3'; P16: F5'-CGCAGGTTCTTGTCACTGT-3'; R 5'-TGTTCACGAAAGCCAGAGCG-3'; P21: F5'-CCTGGT GATGTCCGACCTG-3'; R 5'-CCATGAGCGCATCGC AATC-3'; Ki67: F 5'-ATCATTGACCGCTCCTTTAGGT-3'; R 5'-GCTCGCCTTGATGGTTCCT-3'; TGFβ1: F 5'-CTCCCG TGGCTTCTAGTGC-3'; R 5'-GCCTTAGTTTGGACAGGA TCTG-3'; Smad2: F 5'-TCCGTACCACTACCAGAGAGT-3'; R 5'-GGCGGCAGTTCTGTTAGAATC-3'; Smad3: F 5'-CAC GCAGAACGTGAACACC-3'; R 5'-GGCAGTAGATAACGT GAGGGA-3' and were synthesized by Beijing Tsingke Biotech Co., Ltd.

Single-cell RNA sequencing (scRNA-seq) data. The scRNA-seq data were downloaded from the Genome Sequence Archive (GSA; accession no. CRA010641) of the China National Center for Bioinformation. The subset of dorsal wound healing samples were specifically analyzed for aged (O) vs. young (Y) mice, designated as skin_OD0, skin_OD2, skin_OD4, skin_OD7, skin_YD0, skin_YD2, skin_YD4 and skin_YD7, corresponding to post-wounding days 0, 2, 4 and 7.

Processing and quality control of scRNA-seq data. In order to align reads of raw data and generate feature-barcode matrices, Cell Ranger software (version 4.0.0; 10xgenomics.com/support/software/cell-ranger/downloads) was used to perform preliminary processing of each subset. CellBender software (version 0.2.0; https://github.com/broadinstitute/CellBender) was used to remove possible background RNA bias contamination resulting from technical errors. Then, Seurat R package (5.0.3; https://cran.r-project.org/web/packages/Seurat/) (12) was then used to perform subsequent quality control based on the expression matrix obtained. Cells with a number of detected genes <200 or >7,000, or a proportion of reads mapping to the mitochondrial genome exceeding 20, were excluded from further analysis during the quality control step. Finally, DoubletFinder R package (2.0.4; https://github.com/chris-mcginnis-ucsf/DoubleFinder) was used to identify and filter out potential doublets from the sequencing data in each subset.

Data integration, identification of cell types and differentially expressed genes (DEGs). To effectively merge the eight datasets of interest aforementioned, the Seurat integration algorithm was used. 'NormalizeData', 'FindVariableFeatures' and 'ScaleData' functions from the Seurat R package (5.0.3) were applied to normalize and scale the integrated datasets, following the standard workflow. Principal component analysis (PCA) dimensions were then calculated using the 'RunPCA' function from the Seurat R package (5.0.3). To address batch effects among the eight datasets, the Harmony R package (1.2.0; portals.broadinstitute.org/harmony/) was employed. Cluster identification was performed using the 'FindNeighbors', followed by the 'FindClusters' function with a resolution parameter set to 0.5. For cell type annotation, the 'FindALLMarkers' function was leveraged to identify marker genes and their expression patterns in each cluster. Finally, by mapping the results to the CellMaker 2.0 database (117.50.127.228/CellMarker), 14 distinct cell types were successfully identified.

The 'FindMakers' function was used to identify DEGs between skin_OD0 and skin_YD0, skin_OD2 and skin_YD2, skin_OD4 and skin_YD4, as well as skin_OD7 and skin_YD7 in Fibroblast, which were based on the Wilcoxon test. The screening criteria for DEGs were selected by |log2FC| >0.25 and adjust P-value <0.05.

Gene Ontology (GO) enrichment analysis. To gain insight into the biological functions associated with the previously identified DEGs, the DAVID database (http://david.nicifcrf.

gov/summary.jsp) was used to obtain enriched biological functional annotations of these DEGs. The 'ggplot2' R package (version 3.5.0; ggplot2.tidyverse.org) was used to visualize the results.

Inference of cell-cell communication. The CellChat R package (version 1.6.1; https://github.com/sqjin/CellChat) was used to calculate and exhibit the cell-cell communication pattern between cell types of interest. In brief, CellChat compares sequencing datasets with the CellChatDB dataset to compute the expression levels of ligand-receptor pair across various cell types. Following this, using the 'computeCommunProbPathway' function, it derives the probabilities of intercellular communication based on this expression. Ultimately, the consolidation of these probabilities across distinct communication pathways yields the comprehensive network of intercellular communication.

Cell-cell communication analysis of young and aged wounds. To comprehensively elucidate signaling changes between young and aged wounds, a comparative cell-cell communication pattern was conducted. Initially, CellChat was independently applied to both young and aged datasets to generate distinct CellChat objects and quantify the cell-cell communication pattern between Fibroblast and Endothelia cell in each condition. Subsequently, those two objects were merged and a comparative analysis was employed to detect significant alteration between young and age wounds.

Statistical analysis. Differentially expressed genes (DGEs) among various types of cells were identified. Then filtered DEGs were used to compute communication probabilities and enrichment analysis, such as GO. To evaluate the statistical power of RNA-seq experiments across different cell types, power was calculated using the 'RNASeqPower' package in R (bioconductor.org/packages/release/bioc/html/RNASeqPower). The results showed the RNA-seq power for EC and Fib were 0.982 and 0.926. The data are presented as means ± standard deviations (SD) and the statistical analysis was performed using GraphPad Prism Software (version 9.5; Dotmatics). Significant differences between groups were determined using two-way analysis of variance (ANOVA) followed by Bonferroni post hoc test. $P<0.05$ was considered to indicate a statistically significant difference.

Results

Blood vessel density is decreased in aged wounds. Proper vascularization is essential for effective wound healing, as excessive vascularization may lead to pathological scars, whereas insufficient vascularization can delay healing (13). To investigate the disparities in vascular regeneration between aged and young subjects, we established a murine dorsal wound model. The healing rate was markedly higher in young mice than in aged mice (Fig. 1A and B). This disparity was accompanied by distinct subcutaneous neovascular network patterns: aged wounds exhibited reduced capillary length around wound margins (Fig. 1A and D), whereas young wounds developed robust tubular vascular structures as indicated by H&E staining and CD31/SMA co-staining (Fig. 1C and E). Collectively, these findings demonstrated that vascular regenerative capacity is impaired in aged wounds.

Construction of single-cell transcriptional atlases from young and aged wounds. To gain a comprehensive understanding of the dynamic cellular and molecular differences between young and elderly mice during wound healing, single-cell RNA-sequencing datasets from the Genome Sequence Archive (accession no. CRA010641) were analyzed (14). Specifically, a subset of full-thickness excisional skin wounds was selected, as shown in Fig. 2A. Following dataset integration and rigorous quality control, high-quality sequences were obtained from 73,357 cells across various time points: skin-YD0 (8,618 cells), skin-YD2 (7,253 cells), skin-YD4 (7,690 cells), skin-YD7 (5,830 cells), skin-OD0 (9,333 cells), skin-OD2 (18,820 cells), skin-OD4 (7,624 cells) and skin-OD7 (OD7 9,189 cells). Within this comprehensive cellular atlas (Fig. 2B), 15 distinct cell types were identified, including Fibs (Fib, $Dpt^{Hi}Pdgfra^{+}Col4a^{+}$) (15), ECs (Ec, $Ptprb^{+}Pecam1^{+}Sox17^{+}$) (16), papillary Fibs (Fp, $Lef1^{+}$), smooth muscle cells (SMC, $Lmod1^{+}Pln^{+}Acta2^{Hi}$) (17), fascia cells (Fasc, $Pax7^{+}Erfe^{+}Gpx3^{Hi}$), type 1 macrophages (Mac1, $Stat1^{Hi}$ $Arg1^{Lo}$), type 2 macrophages (Mac2, $Arg1^{Hi}$), neutrophils (Neu, $S100a8^{Hi}S100a9^{Hi}$), lymphocytes (Lym, $Cd3d^{Hi}Cd3g^{Hi}$), T cells (T-cell, $Trat1^{+}Cd3g^{Hi}Cd3e^{Hi}Cd3d^{Hi}Nkg7^{Hi}$) (18), suprabasal cells (Supra $Krt6a^{+}Krt6b^{+}$) (19), spinous and granular keratinocytes (Spin, $Krt1^{Hi}$), basal keratinocytes (Basal, $Krt5^{Hi}$) (20), epithelial cells (Epi, $Krt79^{Hi}$) (21) and germinative layer cells (Germ, $Ube2c^{Hi}$), based on top marker expression (Fig. 2C-F).

Next, these cell types and their alterations during wound healing were comprehensively analyzed. As shown in Fig. 3A, inflammatory cells were the predominant cell type across the two groups, with Mac1 at 31.17%, Mac2 at 7.62%, Neu at 16.51%, Lym at 2.22% and T-cell at 0.79%. Consistent with this, a classical inflammatory infiltration-to-resolution process was observed in both groups (Fig. 3B-D). The distribution of ECs clearly differed between the two groups, with young wounds exhibiting markedly higher cell numbers across all time points. Young wounds exhibited a faster recovery rate in terms of Fib count (Fig. 3B-F). Fp, known to promote hair follicle formation (22,23), were predominantly observed in OD0 (Fig. 3B-D). These findings of impaired EC restoration and delayed Fib recovery underscore the diminished regenerative capacity and compromised healing potential of aged tissues.

Dynamic molecular alterations in ECs and Fibs during wound healing in young and aged wounds. To gain a deeper insight into the transcriptomic changes in ECs and Fibs throughout the healing process in both young and aged mice, ECs and Fibs were extracted and differentially expressed genes (DEGs) identified at four time points, as shown in Figs. 3G-J and 4A-D.

On day 0, regulator of G protein signaling 5 (*Rgs5*), a recognized marker of endothelial function and vascular remodeling (24) and platelet-derived growth factor A (*Pdgfr*), which is critical for vascular development (25), were downregulated specifically in aged wounds ECs. Concurrently, chronic inflammation-related genes, including cytochrome

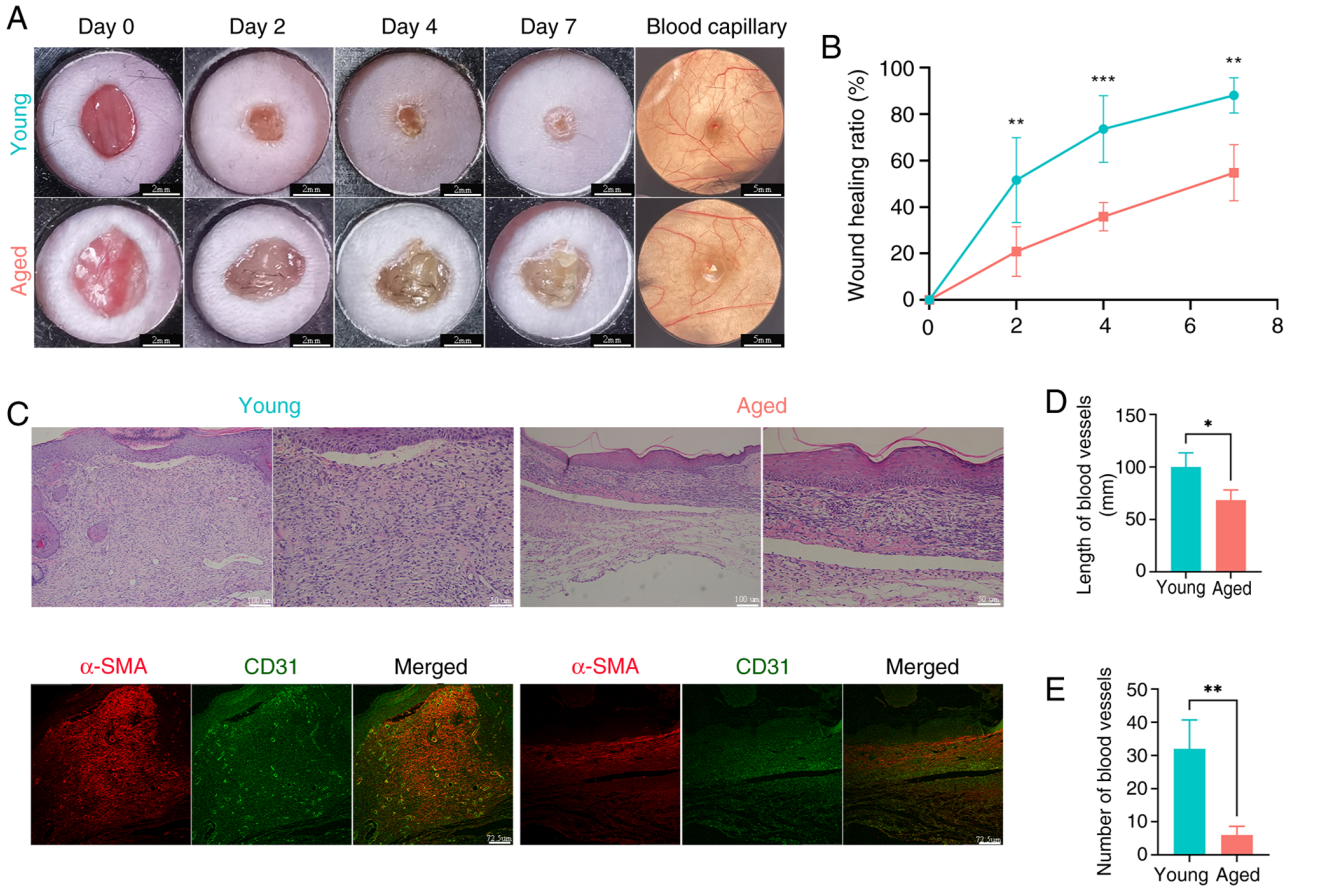

Figure 1. Decreased vascularization in wound healing associated with aging. (A) Representative images of cutaneous wounds in two age groups (aged vs. young) of mice on days 0, 2, 4 and 7; and the blood capillaries at the wound site at day 7. (B) Quantification of the wound healing rate after injures in young and aged mice. (young: n=5, aged: n=3), (C) H&E staining and immunohistochemical profiles of CD31 and α-SMA in young vs. aged wounds at day 7 post-injury. (D and E) Quantification of subcutaneous blood vessels length (D) and density (E) in aged vs. young wounds, *P<0.05, **P<0.01, ***P<0.001. H&E, hematoxylin and eosin; CD, cluster of differentiation; α-SMA, α-smooth muscle actin.

P450 1A1 (*Cyp1a1*) and angiopoietin-like protein 4 (*Angptl 4*) (26,27), were upregulated in aged wounds ECs (Fig. 3G). On days 2 and 4, significant DEGs (highlighted in red in the figure) were relatively sparse, probably reflecting reduced EC populations. However, *S100a8*, *IL1b* and *Cdkn2b*, factors related to the regulation of inflammation and aging (28), remained upregulated in aged wounds ECs (Fig. 3H and I). Notably, mitochondrial genes critical for metabolism, including *mt-Atp8*, *mt-Nd3* and *mt-Nd4*, were downregulated. Notably, platelet-derived growth factor receptor-β (*Pdgfrb*), essential for endothelial differentiation (29), was markedly downregulated in aged wounds ECs on day 7 (Fig. 3J). Most of the upregulated DEGs on day 7, such as *H2-Ab1*, *H2-Eb1*, *H2-Aa* and *Cd74*, were related to immune activation and antigen presentation (30).

Dynamic transcriptomic changes in Fibs are critical for wound healing progression (31). As shown in Fig. 4A, on day 0, uninjured aged skin exhibited significant downregulation of key Fib markers, including adenylate cyclase 1 (*Adcy1*; myoFib activation), collagen type I α 1 (*Col1a1*; fibrosis driver) and Fib growth factor receptor 4 (*Fgfr4*; proliferation/migration) (32). On days 2-4, genes associated with tissue aging and chronic inflammation, including *S100a8*, *cd74 cd52*, *Ccl6* and *S100a4*, were upregulated in aged wound Fibs (Fig. 4B and C). By day 7, delta-like homolog-1 (*Dlk-1*; adipogenesis inhibitor), elastin (*Eln*; extracellular matrix components), renin-angiotensin-aldosterone system (*RAAS*; fibrosis-related genes) and angiotensin II receptor 1A (*Agtr1a;* transcription growth factor (TGF)-β signaling pathway) were markedly downregulated (33-36).

The present study identified 31 genes that were consistently and markedly downregulated in aged vs. young wounds across all time points (Fig. 4 E), including fibrosis-associated genes (*Meg3*, *Sparc*, *Nrp1* and *Peg3*) (37-40). To elucidate the biological significance of these alterations, Gene Ontology (GO) term enrichment analysis was performed. Downregulated DEGs in both uninjured skin and healing aged skin were consistently markedly associated with cell proliferation, cell division and angiogenesis (Fig. 4G-J).

Intercellular communication pattern differences between aged and young wounds. Using CellChat, distinct intercellular communication patterns were identified in the two age groups. Given the similarity in principal cell types and the more representative wound differences on day 7, the OD7 and YD7 datasets were selected for analysis. First, the two datasets were integrated to construct a unified cell communication network, categorized into four functional clusters (Fig. 5A and B). Pathways involving IL2, IL4, WNT and BMP clustered together, suggesting their universal roles in wound healing.

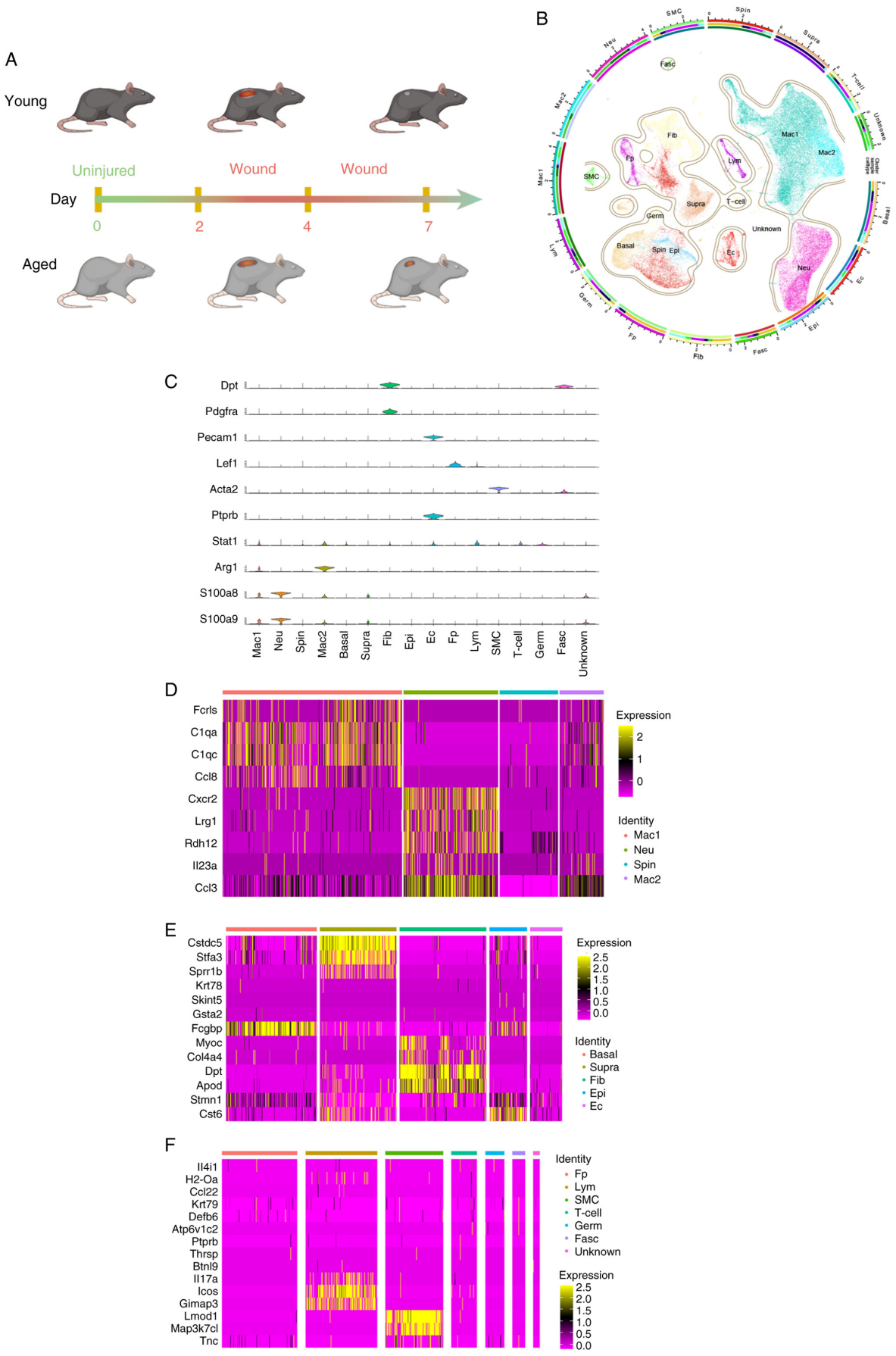

Figure 2. The visualization and analysis of the single-cell transcriptional atlas. (A) Schematic diagram illustrating the study workflow for single-cell RNA sequencing datasets (GSA: CRA010641) across different time points. (B) Cirlize plot visualizing the UMAP of cell types in young and aged wounds across four time points. Colors represent cell types. (C-E) Expression of maker genes used for identification of cell types in (B). (F) Heatmap of top three differentially expressed marker genes of cell types in (B). GSA, Genome Sequence Archive; UMAP, uniform manifold approximation and projection.

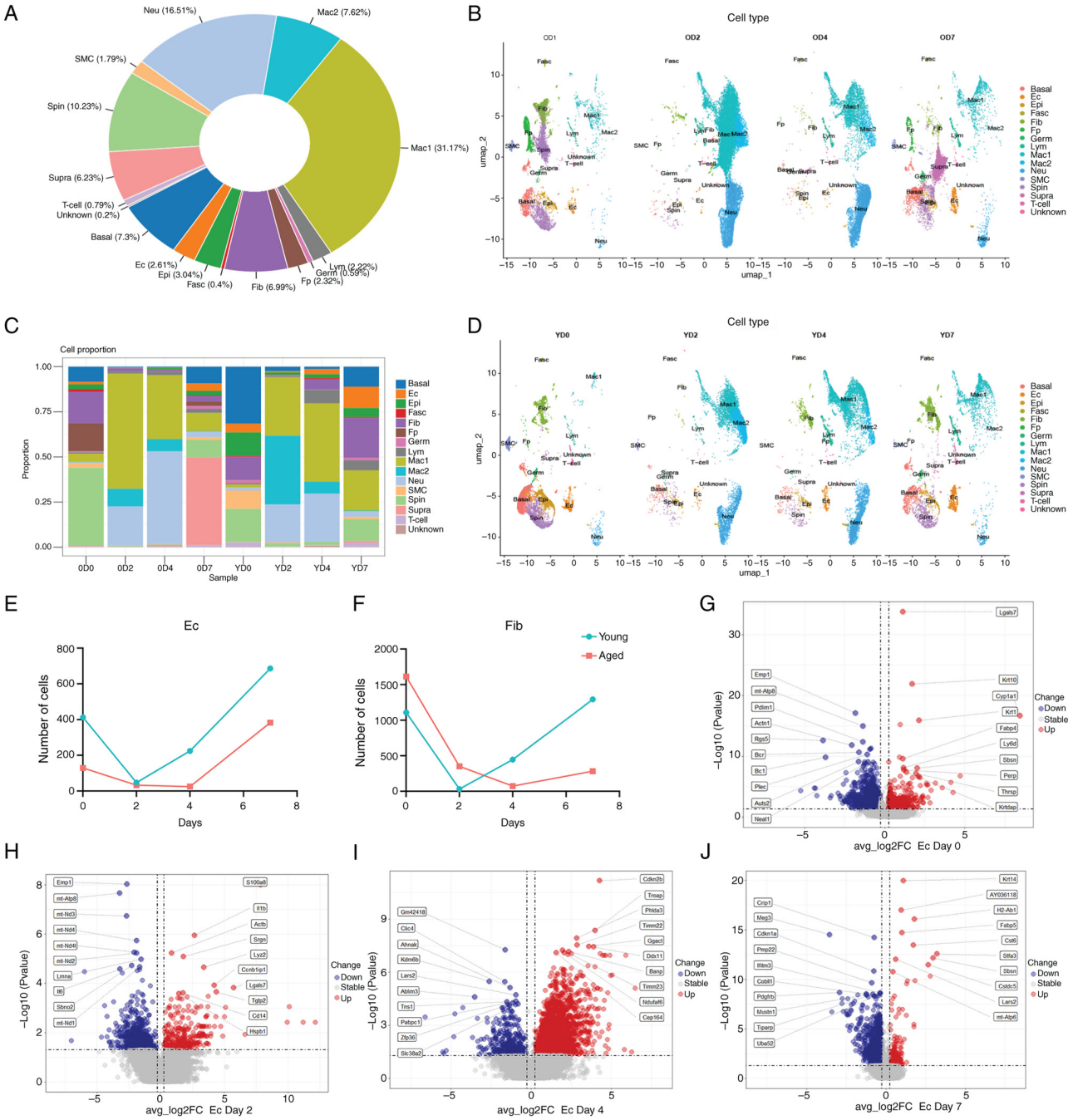

Figure 3. Cellular composition alterations between young and aged wounds. (A) Proportion of all cell types in wounds from the integrated datasets. (B) UMAP of each cell types in aged wound over four time points. (C) Proportion of cell types in young and aged wounds over time points. (D) UMAP of each cell types in young wound over four time points (E) Quantification of the Ec in young and aged wounds over time points. (F) Quantification of the Fib in young and aged wounds over time points. Volcano plots of differentially expression genes of EC in aged compared with young wounds at day (G) 0, (H) 2, (I) 4 and (J) 7. UMAP, uniform manifold approximation and projection; OD0, aged wound at day 0; OD2, aged wound at day 2; OD4, aged wound at day 4; OD7. aged wound at day 7; YD0, young wound at day 0; YD2, young wound at day 2; YD4, young wound at day 4; YD7, young wound at day 7; Ec, endothelial cell; Fib, fibroblast.

By contrast, the CCL, GDF, PERIOSTIN, ACTIVIN, TGF-β and NRG pathways formed distinct clusters, highlighting their differential contributions to age-related healing outcomes (Fig. 5B).

These pathways demonstrated substantial divergence in Euclidean distances within the shared two-dimensional space (Fig. 5C). Of 52 pathways, 16 showed significant activity in information flow analysis, albeit with varying intensities (Fig. 5D). A total of three pathways were markedly upregulated in OD7: midkine (inflammation/tissue repair regulator) (41,42), CCL (inflammatory pathway;) (43) and TGF-β (wound healing/fibrosis mediator) (44-46).

Age-related differences in cell type-specific communication were pronounced. Aged wounds exhibited reduced incoming interaction strength for ECs and Fibs when compared with young wounds (Fig. 5E and F). After consolidation and standardization, Fibs displayed the most pronounced signal strength alterations in both incoming and outgoing communications, while ECs also showed substantial variations (Fig. 5G). These findings indicate that intercellular communication,

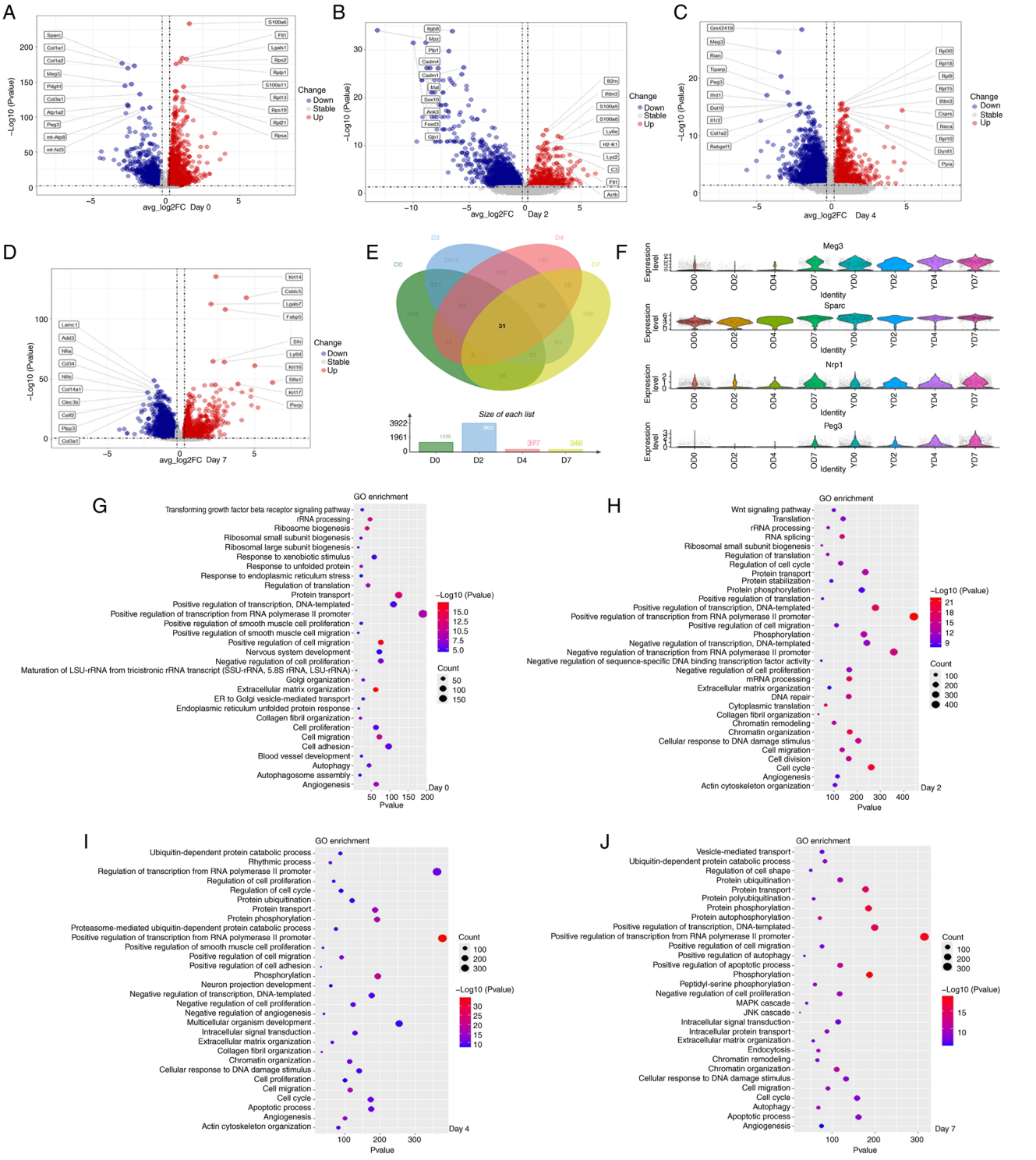

Figure 4. Differential expression genes analysis of Fib in age compared with young wounds. Volcano plots of DEGs at days (A) 0, (B) 2, (C) 4 and (D) 7. (E) Venn diagrams showing the overlap of downregulated DEGs at days 0, 2, 4 and 7. Each section displays the number of DEGs. (F) Expression patterns of Meg3, Sparc, Nrp1 and Pdgfrl. GO term analysis of downregulated DEGs at days (G) 0, (H) 2, (I) 4 and (J) 7. Fib, fibroblast; DEGs, differentially expression genes; GO, Gene Ontology.

particularly between ECs and Fibs, is markedly decreased in elderly wounds.

Pathway-specific visualization revealed the key contributors to communication differences (Fig. 5H-J). In Fibs, the diminished incoming signal intensity in aged wounds primarily involved the Wnt, EGF, TGF-β, GAS, IL-6, PROS and Fas ligand (FASLG) pathways. Similarly, ECs exhibited reduced incoming signals primarily via the Wnt, TGF-β and FASLG pathways, which were all upregulated in YD7.

Comparative analysis of altered signaling interaction between ECs and Fibs in aged vs. young wounds. To investigate age-related differences in EC-Fib communication during wound healing, CellChat was employed to quantify the differences

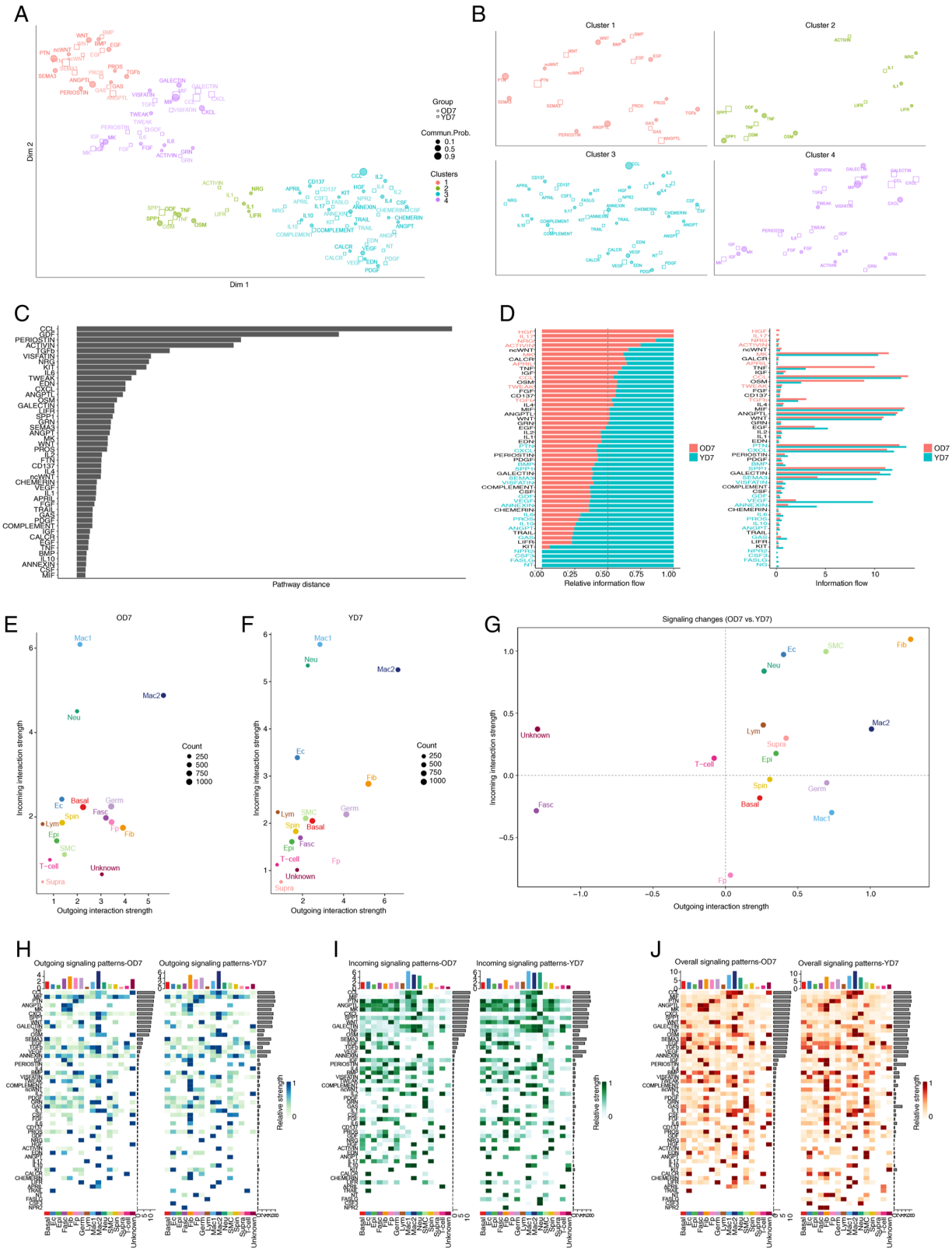

Figure 5. Differential intercellular communication patterns between aged and young wounds. (A) Clustering signaling pathways from aged and young wounds at day 7 into a shared two-dimensional manifold. (B) Magnified view of each pathway cluster. (C) The overlapping signaling pathways between aged and young wounds at day 7 were ordered in accordance with their pairwise Euclidean distance in the shared two-dimensional manifold. (D) The depiction of all signaling pathways within the overall information flow of the inferred networks between aged and young wounds at day 7. The signaling pathways colored red are more enriched in aged wound. The signaling pathways colored green are more enriched in young wound. The signaling pathways colored black are equally enriched between aged and young wounds at day 7. (E) Interaction analysis across all cell types in the aged wound at day 7 identifying prominent signaling sources and targets. (F) Interaction analysis across all cell types in the young wound at day 7 identifying prominent signaling sources and targets. (G) Altered signaling pathways across all cell types in aged compared with young wounds at day 7. (H) Heatmap of all signaling pathways across all cell types between aged and young wounds at day 7, focusing on outgoing signaling patterns. (I) Heatmap of all signaling pathways among all cell types between aged and young wounds at day 7, emphasizing incoming signaling patterns. (J) Heatmap of all signaling pathways among all cell types in aged vs. young wounds at day 7. OD7. aged wound at day 7; YD7, young wound at day 7.

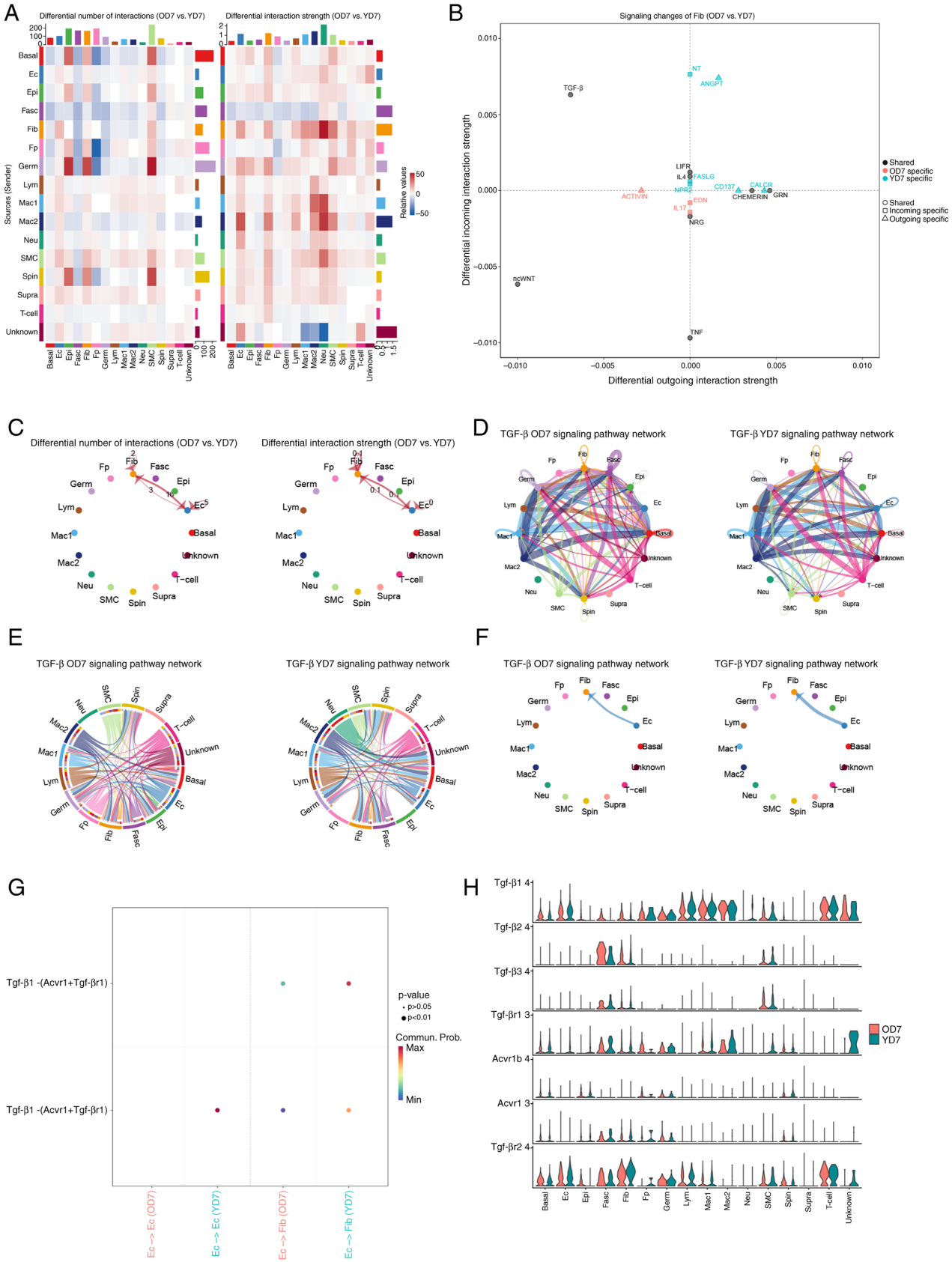

Figure 6. Altered signaling interaction between Fib and Ec in aged vs. young wounds. (A) Differences in interaction numbers and strength across all cell types in aged compared with young wounds at day 7. (B) Altered signaling pathways associated with Fib in aged compared with young wounds at day 7. (C) Difference in interaction numbers and strength specifically between Fib and Ec in aged vs. young wounds at day 7. (D) Circle plot of TGF-β pathway-associated interaction network across all cell types in aged and young wounds at day 7. (E) Chord diagrams of TGF-β pathway-associated interaction network across all cell types in aged and young wounds at day 7. (F) The strength of interaction from Ec to Fib via TGF-β pathway in in aged and young wounds at day 7. The thickness of the connecting line indicates the level of communication probability. (G) Significant ligand-receptor pairs that contribute to the signaling sent from EC via TGF-β pathway in in aged and young wounds at day 7. (H) The distribution of gene expression related to the TGF-β pathway across all cell types in in aged and young wounds at day 7. OD7. aged wound at day 7; YD7, young wound at day 7; TGF-β, transforming growth factor β; Ec, endothelial cell; Fib, fibroblast.

in communication probabilities between OD7 and YD7. As shown in Fig. 6A, young wounds exhibited markedly increased numbers and strength of EC-Fib interactions compared with aged wounds, regardless of signal origin. Network analysis corroborated the distinct communication patterns: Young wounds showed 16 novel Fib-EC interactions and three additional EC-Fib connections compared with aged wounds, accompanied by enhanced interaction strength (Fig. 6C).

Pathway analysis revealed significant differences in Fib-related signaling pathways between the age groups. Notably, the TGF-β pathway demonstrated divergent regulation in young wounds, with increased incoming but decreased outgoing signaling from Fibs (Fig. 6B). Further examination of the entire TGF-β pathway network revealed enhanced EC-EC communication, a feature absent in aged tissue (Fig. 6D). Moreover, young ECs exhibited broader signaling versatility, functioning as both signal senders and receivers, whereas aged ECs primarily acted as signal sources (Fig. 6E). Notably, EC-Fib communication via TGF-β was substantially augmented in young wounds (Fig. 6F), mediated via enhanced signaling through Acvrl-TGF-βR1and TGF-βR1-TGF-βR2 ligand-receptor pairs (Fig. 6G). Mechanistically, the age-related downregulation of TGF-β1 on ECs and TGF-βR2on Fibs probably contribute to impaired TGF-β signaling in aged wounds (Fig. 6H).

Together, these findings demonstrate the age-dependent dysregulation of EC-Fib communication, particularly via TGF-β signaling. This impaired crosstalk may underline the delayed healing kinetics in aged wounds.

Co-culture reveals impaired interaction between ECs and Fibs in aged wounds. To verify the impaired interaction between ECs and Fibs through the TGF-β pathway in aged wounds, we induced Fib senescence via high-glucose treatment *in vitro* and evaluated the effects of ECs on young Fibs vs. aged Fibs through Transwell-based indirect co-culture system. First, a senescent Fib model was established by culturing primary mouse dermal fibroblasts in gradient concentrations of high-glucose medium (50 and 75 mmol/l) to determine the optimal senescence-inducing dose. qPCR analysis revealed that the senescence marker genes *P16* and *P21* were markedly upregulated, while the proliferation marker gene *Ki67* was markedly downregulated in high-glucose groups (Fig. 7A-C). Protein-level validation via immunofluorescence demonstrated that the 75 mmol/l high-glucose group exhibited markedly higher senescence protein markers and reduced proliferative capacity compared with normal glucose controls (Fig. 7D-G). These results confirmed the successful establishment of the senescent Fib (old) model *in vitro*. Based on these findings, Fib (old) showing the most pronounced senescence phenotype from the 75 mmol/l high-glucose group was selected for subsequent experiments.

Following 3 days of co-culture with ECs, senescent Fibs (Fib-old) displayed significant downregulation of *TGFβ1*, *Smad2* and *Smad3* genes, critical fibrotic markers in the TGFβ signaling pathway, which was further confirmed by immunofluorescence staining (Fig. 7H-R).

Discussion

Delayed wound healing in elderly patients correlates with diminished vascularization and cellular dysfunction; however, the molecular mechanisms involving ECs and Fibs remain poorly defined. Using a murine dorsal wound model, the present study observed delayed healing and reduced subcutaneous capillary regeneration in aged mice vs. young controls, as indicated by H&E and dual-labeled immunohistochemical staining. To gain deeper insights into these processes, the present study used comprehensive single-cell transcriptomic atlases in conjunction with CellChat to meticulously analyze the characteristic alterations and interaction disparities in Fibs and ECs during wound healing. It thus identified potential therapeutic targets for addressing wounds in the elderly, offering new avenues for research and clinical interventions.

Angiogenesis plays a critical role during the proliferative phase of wound healing by restoring blood flow, with young wounds exhibiting robust vascular network formation through this process (47). However, aging markedly impairs vascular regenerative capacity, as demonstrated by reduced EC proliferation rates in aged wounds (48,49). The findings of the present study align with this paradigm: Aged mice exhibited markedly diminished vascular regeneration at wound margins compared with young controls as indicated by histological assessment and single-cell transcriptomic profiling. Notably, genes associated with angiogenesis, such as *Rgs5* and *Pdgfr*, were strongly downregulated in ECs in aged wounds, whereas the upregulated genes, including *mt-Atp8*, *mt-Nd3*, *S100a8*, *IL1b*, *Cdkn2b* and *mt-Nd4*, were intricately associated with chronic inflammation and the natural aging process (50). These findings not only underscored the challenges posed by aging in wound healing but also highlighted the need for further research into potential therapeutic strategies that can counteract this age-related decline in vascular regeneration.

Fib regeneration and functional plasticity are fundamental to effective wound healing. The present study demonstrated that Fibs in aged wounds exhibit markedly impaired regenerative capacity, which may contribute to the delayed and inefficient healing observed in elderly populations. Molecular profiling revealed critical dysregulation: Fibs in aged wounds showed marked downregulation of genes governing cell activation, proliferation, migration and fibrotic remodeling, which are key pathways that could be therapeutically targeted to restore healing competence. Concurrently, *S100a8*, *CD74*, *CD52*, *CCL6* and *S100a4* were upregulated in aged Fibs, mirroring pro-inflammatory signatures previously observed in aged ECs, indicating a conserved inflammatory activation state across stromal cell types in aged tissue. This persistent inflammatory phenotype, exacerbated by aging itself, properly perpetuates a microenvironment hostile to tissue repair (51,52). GO analysis reinforced these observations, revealing age-related declines in Fib functions essential for healing, including collagen secretion, migratory capacity and vascular support, which collectively explain the suboptimal clinical outcomes in elderly wound healing.

Wound healing relies on precise cellular crosstalk; hence, communication failures can drive pathological extremes such as chronic, non-healing wounds or excessive scarring (53). Through systematic analysis of day-7 communication networks, six dysregulated pathways (CCL, GDF, PERIOSTIN, ACTIVIN, TGF-β, NRG) that underlie impaired healing in aged tissues were identified. Notably, analysis revealed striking age-related disparities in Fib signaling patterns, with

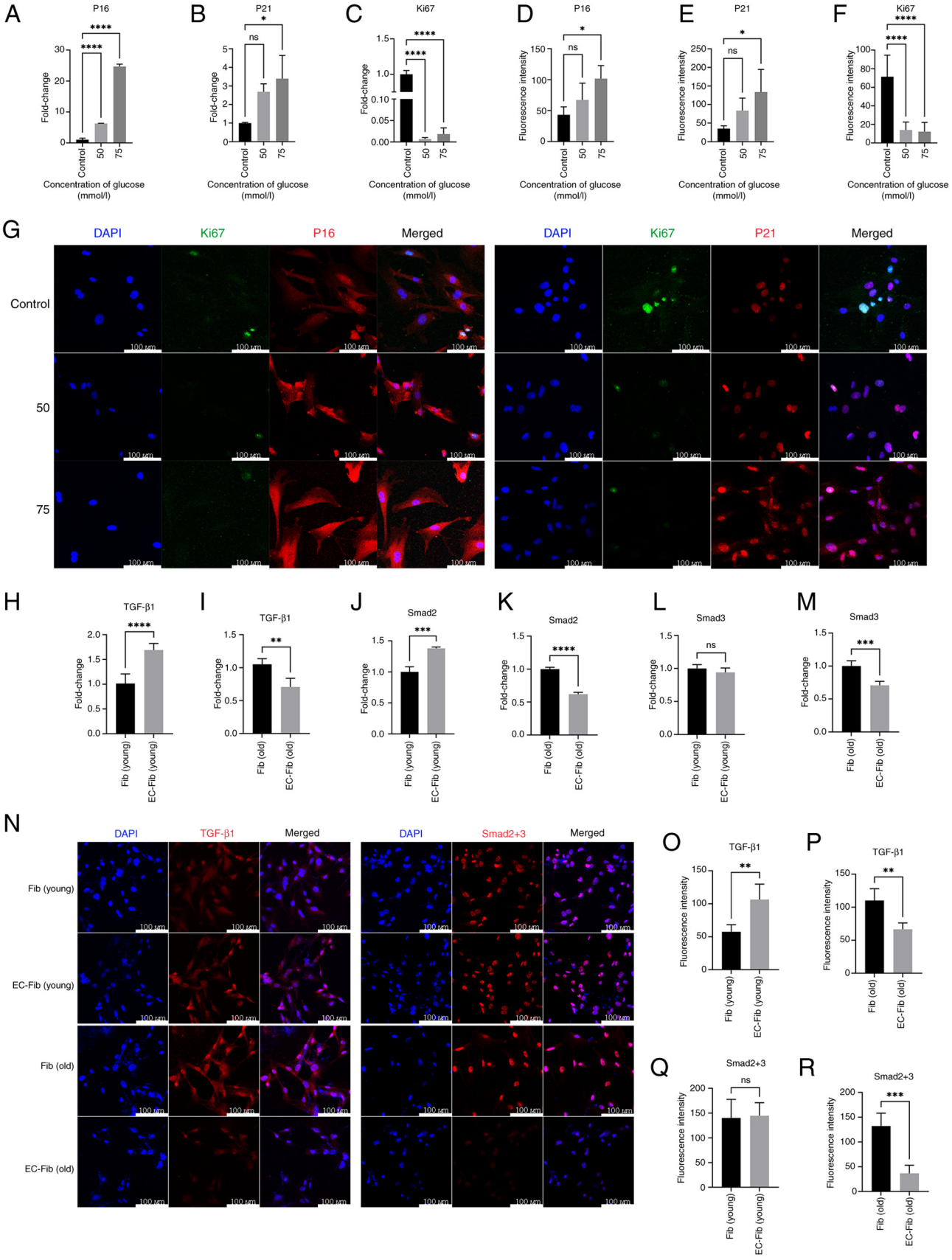

Figure 7. Gene and protein expression profiling in fibroblasts under high-glucose induction and co-culture system. Gene expression level of (A) *P16*, (B) *P21* and (C) *Ki67* in fibroblasts under different glucose concentrations. (n=3) Quantification of fluorescence intensity for (D) P16, (E) P21 and (F) Ki67 in fibroblasts under different glucose concentrations following (G) Immunofluorescence staining. (H) *TGF-β1* gene expression in young fibroblasts co-cultured with ECs. (I) *TGF-β1* gene expression in old fibroblasts co-cultured with ECs. (J) *Smad2* gene expression in young fibroblasts co-cultured with ECs. (K) *Smad2* gene expression in old fibroblasts co-cultured with ECs. *Smad3* gene expression in (L) young fibroblasts co-cultured with ECs. (M) *Smad3* gene expression in old fibroblasts co-cultured with ECs. (N-R) Immunofluorescence staining and quantification of fluorescence intensity for TGF-β1 and Smad2+3 in fibroblasts under different co-culture system. *P<0.05, **P<0.01, ***P<0.001, ****P<0.0001.

distinct pathway activation profiles in aged compared with young wounds that critically influence healing outcomes (54). Focusing on the interplay between ECs and Fibs, a significant reduction in their communication strength was found. By analyzing specific changes in signaling patterns and intensities, it was determined that the decrease in EC-Fib interaction in elderly wounds was primarily mediated via the TGF-β pathway, which plays a crucial role in all phases of wound healing by regulating cell proliferation, migration, extracellular matrix production and the immune response (53,55). Critically, these computational predictions were experimentally validated in an *in vitro* co-culture system, where senescence-induced Fibs exhibited significant downregulation of TGF-β1 expression and reduced SMAD2/3 (key downstream effectors of TGF-β signaling), paralleling the fibrotic pathway suppression observed in aged wounds. Therefore, the present study provided novel insights into the delayed wound healing process in the elderly, specifically focusing on EC-Fib interaction. Additionally, consistently and markedly downregulated DEGs were identified, including *Meg3*, *Sparc*, *Nrp1* and *Peg3*. These genes are closely associated with tissue fibrosis and play pivotal roles in pathophysiological processes either directly or by interacting with the TGF-β pathway (56-59). It is hypothesized that these downregulated DEGs may play critical roles within the TGF-β pathway, potentially explaining delayed wound healing in the elderly. However, further experimental evidence is required to validate this hypothesis.

The present study systematically investigated EC-Fib interactions, elucidating their regenerative dynamics, phenotypic plasticity, with a particular focus on age-associated cellular communication deficits during wound healing. This work not only advanced our understanding of geriatric wound pathophysiology but also established a framework for developing targeted therapies against age-related healing impairments. Notably, while cellular senescence, a cardinal feature of aging, has been shown to activate TGF-β signaling, promoting fibrotic responses in certain contexts (60), the present study revealed a paradoxical mechanism in aged wounds. Specifically, it demonstrated the functional impairment of the TGF-β-mediated EC-Fib communication axis in aging tissues, which appears mechanistically linked to healing deficiencies. These findings challenged the prevailing fibrosis-centric paradigm and uncover new dimensions in understanding multicellular crosstalk within the geriatric wound niche.

Acknowledgements

The authors would like to thank Professor Guanghua Liu (State Key Laboratory of Membrane Biology, Chinese Academy of Sciences, Beijing, China) for providing data support.

Funding

The present study was supported by the Beijing Natural Science Foundation (grant no. L234066), National Key Research and Development Program of China (grant nos. 2022YFA1104600 a nd 2022YFA1104604), the National Nature Science Foundation of China (grant nos. 92268206, 82274362 and U24A20374), the CAMS Innovation Fund for Medical Sciences (CIFMS; grant no. 2019-I2M-5-059), the Military Medical Research Projects (grant nos. 2023-JSKY-SSQG-006, 2023-JSKY-SSQG-008 an d 2023-JCJQ-ZD-117-12), the Science Fund for National Defense Distinguished Young Scholars (grant no. 2022-JCJQ-ZQ-016), Youth Independent Innovation Science Fund Project of PLA General Hospital (grant no. 22QNFC018) and Innovation Cultivation Fund of the Sixth Medical Center, Chinese PLA General Hospital (grant no. CXPY202210).

Availability of data and materials

The data generated in the present study are included in the figures of this article. The raw scRNA-seq data are available in the Genome Sequence Archive (GSA: CRA010641; https://ngdc.cncb.ac.cn/gsa/search?searchTerm=CRA010641) of the China National Center for Bioinformation.

Authors' contributions

JL conceived the present study. DZ conducted bioinformatics analysis. MZ and LL performed the animal experiments. YH, XG collected bioinformatics data. ZL and YK conceived and executed *in vitro* cytological experiments (including endothelial cell-fibroblast co-culture systems and age-related cell senescence assays), interpreted the corresponding data, and co-wrote the methodology section. XF and SH contributed to the study conception and design, critically revised the manuscript (including restructuring the logical framework and validating mechanistic insights), and secured financial support for the project. DZ and XG confirm the authenticity all the raw data. All authors have read and approved the final manuscript.

Ethics approval and consent to participate

All animal experiments and protocols involving surgical procedures were approved by the Institutional Animal Care and Use Committee of the Chinese PLA General Hospital in Beijing, China, under approval number 2023-407-01. These experiments and protocols fully complied with the regulatory requirements outlined in the ARRIVE guidelines and adhered to the euthanasia guidelines published by the American Veterinary Medical Association in 2020 (61).

Patient consent for publication

Not applicable.

Competing interests

The authors declare that they have no competing interests.

References

1. Tan Y, Zhang M, Kong Y, Zhang F, Wang Y, Huang Y, Song W, Li Z, Hou L, Liang L, *et al*: Fibroblasts and endothelial cells interplay drives hypertrophic scar formation: Insights from in vitro and in vivo models. Bioeng Transl Med 9: e10630, 2023.
2. Sun X, Nkennor B, Mastikhina O, Soon K and Nunes SS: Endothelium-mediated contributions to fibrosis. Semin Cell Dev Biol 101: 78-86, 2020.
3. Ramasamy SK, Kusumbe AP and Adams RH: Regulation of tissue morphogenesis by endothelial cell-derived signals. Trends Cell Biol 25: 148-157, 2015.

4. Sgonc R and Gruber J: Age-related aspects of cutaneous wound healing: A mini-review. Gerontology 59: 159-164, 2013.
5. Brauer E, Lange T, Keller D, Görlitz S, Cho S, Keye J, Gossen M, Petersen A and Kornak U: Dissecting the influence of cellular senescence on cell mechanics and extracellular matrix formation in vitro. Aging Cell 22: e13744, 2023.
6. Dańczak-Pazdrowska A, Gornowicz-Porowska J, Polańska A, Krajka-Kuźniak V, Stawny M, Gostyńska A, Rubiś B, Nourredine S, Ashiqueali S, Schneider A, *et al*: Cellular senescence in skin-related research: Targeted signaling pathways and naturally occurring therapeutic agents. Aging Cell 22: e13845, 2023.
7. Yu GT, Monie DD, Khosla S, Tchkonia T, Kirkland JL and Wyles SP: Mapping cellular senescence networks in human diabetic foot ulcers. Geroscience 46: 1071-1082, 2024.
8. Pilkington SM, Bulfone-Paus S, Griffiths CEM and Watson REB: Inflammaging and the Skin. J Invest Dermatol 141 (4S): 1087-1095, 2021.
9. Ding X, Kakanj P, Leptin M and Eming SA: Regulation of the Wound Healing Response during Aging. J Invest Dermatol 141 (4S): 1063-1070, 2021.
10. Zhou S, Li Z, Li X, Ye Y, Wang M, Jiang J, Tao L, Wang Y, Tung CT, Chung Y, *et al*: Crosstalk between endothelial cells and dermal papilla entails hair regeneration and angiogenesis during aging. J Adv Res 70: 339-353, 2025.
11. Reed MJ and Edelberg JM: Impaired angiogenesis in the aged. Sci Aging Knowledge Environ 2004: pe7, 2004.
12. R Core Team: R: A language and environment for statistical computing. R Foundation for Statistical Computing, Vienna, 2023. http://www.R-project.org/.
13. Martin P and Nunan R: Cellular and molecular mechanisms of repair in acute and chronic wound healing. Br J Dermatol 173: 370-378, 2015.
14. Cai Y, Xiong M, Xin Z, Liu C, Ren J, Yang X, Lei J, Li W, Liu F, Chu Q, *et al*: Decoding aging-dependent regenerative decline across tissues at single-cell resolution. Cell Stem Cell 30: 1674-1691.e8, 2023.
15. Arostegui M, Scott RW, Böse K and Underhill TM: Cellular taxonomy of Hic1+ mesenchymal progenitor derivatives in the limb: From embryo to adult. Nat Commun 13: 4989, 2022.
16. Liu M, Zhang L, Marsboom G, Jambusaria A, Xiong S, Toth PT, Benevolenskaya EV, Rehman J and Malik AB: Sox17 is required for endothelial regeneration following inflammation-induced vascular injury. Nat Commun 10: 2126, 2019.
17. Perisic Matic L, Rykaczewska U, Razuvaev A, Sabater-Lleal M, Lengquist M, Miller CL, Ericsson I, Röhl S, Kronqvist M, Aldi S, *et al*: Phenotypic modulation of smooth muscle cells in atherosclerosis is associated with downregulation of LMOD1, SYNPO2, PDLIM7, PLN, and SYNM. Arterioscler Thromb Vasc Biol 36: 1947-1961, 2016.
18. Ng SS, De Labastida Rivera F, Yan J, Corvino D, Das I, Zhang P, Kuns R, Chauhan SB, Hou J, Li XY, *et al*: The NK cell granule protein NKG7 regulates cytotoxic granule exocytosis and inflammation. Nat Immunol 21: 1205-1218, 2020.
19. Zhang X, Yin M and Zhang LJ: Keratin 6, 16 and 17-critical barrier alarmin molecules in skin wounds and psoriasis. Cells 8: 807, 2019.
20. Heinzelmann K, Hu Q, Hu Y, Dobrinskikh E, Ansari M, Melo-Narváez MC, Ulke HM, Leavitt C, Mirita C, Trudeau T, *et al*: Single-cell RNA sequencing identifies G-protein coupled receptor 87 as a basal cell marker expressed in distal honeycomb cysts in idiopathic pulmonary fibrosis. Eur Respir J 59: 2102373, 2022.
21. Veniaminova NA, Vagnozzi AN, Kopinke D, Do TT, Murtaugh LC, Maillard I, Dlugosz AA, Reiter JF and Wong SY: Keratin 79 identifies a novel population of migratory epithelial cells that initiates hair canal morphogenesis and regeneration. Development 140: 4870-4880, 2013.
22. Rippa AL, Kalabusheva EP and Vorotelyak EA: Regeneration of dermis: Scarring and cells involved. Cells 8: 607, 2019.
23. Driskell RR, Lichtenberger BM, Hoste E, Kretzschmar K, Simons BD, Charalambous M, Ferron SR, Herault Y, Pavlovic G, Ferguson-Smith AC and Watt FM: Distinct fibroblast lineages determine dermal architecture in skin development and repair. Nature 504: 277-281, 2013.
24. Li Y, Yan H, Guo J, Han Y, Zhang C, Liu X, Du J and Tian XL: Down-regulated RGS5 by genetic variants impairs endothelial cell function and contributes to coronary artery disease. Cardiovasc Res 117: 240-255, 2021.
25. Bartoschek M and Pietras K: PDGF family function and prognostic value in tumor biology. Biochem Biophys Res Commun 503: 984-990, 2018.
26. Kyoreva M, Li Y, Hoosenally M, Hardman-Smart J, Morrison K, Tosi I, Tolaini M, Barinaga G, Stockinger B, Mrowietz U, *et al*: CYP1A1 enzymatic activity influences skin inflammation via regulation of the AHR pathway. J Invest Dermatol 141: 1553-1563.e3, 2021.
27. Qin L, Zhang R, Yang S, Chen F and Shi J: Knockdown of ANGPTL-4 inhibits inflammatory response and extracellular matrix accumulation in glomerular mesangial cells cultured under high glucose condition. Artif Cells Nanomed Biotechnol 47: 3368-3373, 2019.
28. Ye Y, Yang K, Liu H, Yu Y, Song M, Huang D, Lei J, Zhang Y, Liu Z, Chu Q, *et al*: SIRT2 counteracts primate cardiac aging via deacetylation of STAT3 that silences CDKN2B. Nat Aging 3: 1269-1287, 2023.
29. Rolny C, Nilsson I, Magnusson P, Armulik A, Jakobsson L, Wentzel P, Lindblom P, Norlin J, Betsholtz C, Heuchel R, *et al*: Platelet-derived growth factor receptor-beta promotes early endothelial cell differentiation. Blood 108: 1877-1886, 2006.
30. Stables MJ, Shah S, Camon EB, Lovering RC, Newson J, Bystrom J, Farrow S and Gilroy DW: Transcriptomic analyses of murine resolution-phase macrophages. Blood 118: e192-e208, 2011.
31. Liu Y, Ji Y, Jiang R, Fang C, Shi G, Cheng L, Zuo Y, Ye Y, Su X, Li J, *et al*: Reduced smooth muscle-fibroblasts transformation potentially decreases intestinal wound healing and colitis-associated cancer in ageing mice. Signal Transduct Target Ther 8: 294, 2023.
32. Bergmeier V, Etich J, Pitzler L, Frie C, Koch M, Fischer M, Rappl G, Abken H, Tomasek JJ and Brachvogel B: Identification of a myofibroblast-specific expression signature in skin wounds. Matrix Biol 65: 59-74, 2018.
33. Lu HP, Lin CJ, Chen WC, Chang YJ, Lin SW, Wang HH and Chang CJ: TRIM28 regulates Dlk1 expression in adipogenesis. Int J Mol Sci 21: 7245, 2020.
34. Khoury LE, Posthumus M, Collins M, van der Merwe W, Handley C, Cook J and Raleigh SM: ELN and FBN2 gene variants as risk factors for two sports-related musculoskeletal injuries. Int J Sports Med 36: 333-337, 2015.
35. Matsusaka T, Katori H, Inagami T, Fogo A and Ichikawa I: Communication between myocytes and fibroblasts in cardiac remodeling in angiotensin chimeric mice. J Clin Invest 103: 1451-1458, 1999.
36. AlQudah M, Hale TM and Czubryt MP: Targeting the renin-angiotensin-aldosterone system in fibrosis. Matrix Biol 91-92: 92-108, 2020.
37. Zhao J, Bai J, Peng F, Qiu C, Li Y and Zhong L: USP9X-mediated NRP1 deubiquitination promotes liver fibrosis by activating hepatic stellate cells. Cell Death Dis 14: 40, 2023.
38. Guan T, Fang F, Su X, Lin K and Gao Q: Silencing PEG3 inhibits renal fibrosis in a rat model of diabetic nephropathy by suppressing the NF-κB pathway. Mol Cell Endocrinol 513: 110823, 2020.
39. Wu W, Zhou S, Fei G and Wang R: The role of long noncoding RNA MEG3 in fibrosis diseases. Postgrad Med J 100: 529-538, 2024.
40. Du J, Qian T, Lu Y, Zhou W, Xu X, Zhang C, Zhang J and Zhang Z: SPARC-YAP/TAZ inhibition prevents the fibroblasts-myofibroblasts transformation. Exp Cell Res 429: 113649, 2023.
41. Cerezo-Wallis D, Contreras-Alcalde M, Troulé K, Catena X, Mucientes C, Calvo TG, Cañón E, Tejedo C, Pennacchi PC, Hogan S, *et al*: Midkine rewires the melanoma microenvironment toward a tolerogenic and immune-resistant state. Nat Med 26: 1865-1877, 2020.
42. Hayward S, Gachehiladze M, Badr N, Andrijes R, Molostvov G, Paniushkina L, Sopikova B, Slobodová Z, Mgebrishvili G, Sharma N, *et al*: The CD151-midkine pathway regulates the immune microenvironment in inflammatory breast cancer. J Pathol 251: 63-73, 2020.
43. Russell CD, Unger SA, Walton M and Schwarze J: The human immune response to respiratory syncytial virus infection. Clin Microbiol Rev 30: 481-502, 2017.
44. Meng XM, Nikolic-Paterson DJ and Lan HY: TGF-β: The master regulator of fibrosis. Nat Rev Nephrol 12: 325-338, 2016.
45. Lee JH and Massagué J: TGF-β in developmental and fibrogenic EMTs. Semin Cancer Biol 86 (Pt 2): 136-145, 2022.
46. Morikawa M, Derynck R and Miyazono K: TGF-β and the TGF-β family: Context-dependent roles in cell and tissue physiology. Cold Spring Harb Perspect Biol 8: a021873, 2016.
47. DiPietro LA: Angiogenesis and wound repair: When enough is enough. J Leukoc Biol 100: 979-984, 2016.

48. Riggin CN, Weiss SN, Rodriguez AB, Raja H, Chen M, Schultz SM, Sehgal CM and Soslowsky LJ: Increasing vascular response to injury improves tendon early healing outcome in aged rats. Ann Biomed Eng 50: 587-600, 2022.
49. Bonham CA, Kuehlmann B and Gurtner GC: Impaired neovascularization in aging. Adv Wound Care (New Rochelle) 9: 111-126, 2020.
50. Eming SA, Martin P and Tomic-Canic M: Wound repair and regeneration: Mechanisms, signaling, and translation. Sci Transl Med 6: 265sr6, 2014.
51. Fougère B, Boulanger E, Nourhashémi F, Guyonnet S and Cesari M: Chronic inflammation: Accelerator of biological aging. J Gerontol A Biol Sci Med Sci 72: 1218-1225, 2017.
52. Zhao R, Liang H, Clarke E, Jackson C and Xue M: Inflammation in chronic wounds. Int J Mol Sci 17: 2085, 2016.
53. Kiritsi D and Nyström A: The role of TGFβ in wound healing pathologies. Mech Ageing Dev 172: 51-58, 2018.
54. Talbott HE, Mascharak S, Griffin M, Wan DC and Longaker MT: Wound healing, fibroblast heterogeneity, and fibrosis. Cell Stem Cell 29: 1161-1180, 2022.
55. Zhang J, Zheng Y, Lee J, Hua J, Li S, Panchamukhi A, Yue J, Gou X, Xia Z, Zhu L and Wu X: A pulsatile release platform based on photo-induced imine-crosslinking hydrogel promotes scarless wound healing. Nat Commun 12: 1670, 2021.
56. Lu ZZ, Sun C, Zhang X, Peng Y, Wang Y, Zeng Y, Zhu N, Yuan Y and Zeng MS: Neuropilin 1 is an entry receptor for KSHV infection of mesenchymal stem cell through TGFBR1/2-mediated macropinocytosis. Sci Adv 9: eadg1778, 2023.
57. Fan J, Zhang X, Jiang Y, Chen L, Sheng M and Chen Y: SPARC knockdown attenuated TGF-β1-induced fibrotic effects through Smad2/3 pathways in human pterygium fibroblasts. Arch Biochem Biophys 713: 109049, 2021.
58. Nagashima G, Suzuki R, Asai JI, Noda M, Fujimoto M and Fujimoto T: Tissue reconstruction process in the area of peri-tumoural oedema caused by glioblastoma-immunohistochemical and graphical analysis using brain obtained at autopsy. Acta Neurochir Suppl 86: 507-511, 2003.
59. Zhan H, Sun X, Wang X, Gao Q, Yang M, Liu H, Zheng J, Gong X, Feng S, Chang X and Sun Y: LncRNA MEG3 involved in NiO NPs-induced pulmonary fibrosis via regulating TGF-β1-mediated PI3K/AKT pathway. Toxicol Sci 182: 120-131, 2021.
60. O'Reilly S, Tsou PS and Varga J: Senescence and tissue fibrosis: Opportunities for therapeutic targeting. Trends Mol Med 30: 1113-1125, 2024.
61. Percie du Sert N, Hurst V, Ahluwalia A, Alam S, Avey MT, Baker M, Browne WJ, Clark A, Cuthill IC, Dirnagl U, *et al*: The ARRIVE guidelines 2.0: Updated guidelines for reporting animal research. PLoS Biol 18: e3000410, 2020.